# Study of anomalous Spin/CP components on the Higgs coupling to W pairs with the ATLAS detector

Ricardo Barrué
ricardo.barrue@tecnico.ulisboa.pt

Instituto Superior Técnico, Lisboa, Portugal

April 2020

**Abstract**

The measurement of anomalous Spin/CP components in the $HWW$ vertex would be evidence of physics beyond the Standard Model. More specifically, the non-zero measurement of anomalous CP-odd components would entail the existence of a new source of CP-violation that could, perhaps, explain the observed baryonic asymmetry of the Universe. This work studies the ATLAS sensitivity these components, with an integrated luminosity $L = 139$ fb$^{-1}$ at $\sqrt{s} = 13$ TeV. It targets the $WH \rightarrow \ell\nu b\bar{b}$, (with $\ell = e, \mu$) process in the boosted regime, $p_{T_W} > 250$ GeV, where the sensitivity is higher.

After optimization of the event selection, the sensitivity to the SM signal and to BSM signals with anomalous components was studied, by measuring the expected signal strength, $\mu_{exp}$, and the expected significance, $Z_{exp}$. For the Standard Model (SM) signal, $\mu_{exp} = 1.00 \pm 0.41$ and $Z_{exp} = 2.52\sigma$. For signals with anomalous CP-even components, and also for a signal with an anomalous CP-odd component with large coupling, the expected signal strengths are not compatible with their SM value, with $Z_{exp} > 5\sigma$. For a signal with an anomalous CP-odd component with smaller coupling, $\mu_{exp} = 1.54 \pm 0.42$ and $Z_{exp} = 4.04$, compatible with the SM measurement.

A set of angular observables sensitive to the different anomalous components is introduced, showing that the asymmetry in the $\cos\delta^+$observable has a value of $A(\cos\delta^+) = -0.319 \pm 0.12$ for the signal with an anomalous CP-odd component with smaller coupling, and a zero value for SM sample and backgrounds, thus improving the sensitivity to these components.

**Keywords:** Higgs boson, Spin/CP, CP violation, effective field theory, angular observables

## 1. Introduction

The Standard Model (SM) does not explain the observed imbalance between matter and antimatter in the Universe, the so-called baryonic asymmetry. This imbalance requires not only the existence of CP violation [1], but also a larger amount than that predicted in the SM [2]. In the SM, it appears in the quark sector, arising from complex phases in the Cabbibo-Kobayashi-Maskawa matrix, which relates weak eigenstates with mass eigenstates (solutions of the equations of motion). Thus, in order to explain this imbalance, it is necessary to look for additional sources of CP violation beyond the SM.

This work concerns the study of the tensor structure of the interaction between the Higgs boson and $W$ boson pairs ($HWW$), namely the sensitivity to anomalous (not predicted in the SM) Spin/CP components in the interaction vertex, with a focus on CP-odd components. A measurement of the latter would entail the existence of CP violation in the Higgs sector and would be an evidence of BSM physics. Anomalous components in this vertex lead to modifications to the cross-section of Higgs boson production via vector boson fusion and associated $WH$ production modes, modifying also the shape of kinematic distributions such as the transverse momenta of the $W$ and Higgs bosons, which are pushed to higher values. The sensitivity to these components is thus expected to increase, when targeting higher transverse momenta of the $W$ and Higgs bosons.

The CMS Collaboration performed a study of the tensor structure of the $HVV$ interaction, with $VV = WW, ZZ, Z\gamma, \gamma\gamma$ and $gg$ [3]. The Leading Order (LO) SM couplings for $W$ and $Z$ bosons are assumed equal, $a_1^{WW} = a_1^{ZZ}$, as well as the couplings of the anomalous components, $a_2^{WW} = a_2^{ZZ}, a_3^{WW} = a_3^{ZZ}$. The measured quantities were the effective cross-section ratios and phases and the obtained results were compatible with the SM predictions, showing no evidence for CP violation in this vertex. The ATLAS Collaboration performed measurements of the $VH(H \rightarrow b\bar{b})$ process as a function of the vector boson transverse momentum, $p_{T_V}$, in the Simplified Template Cross Section framework [4]. The measured cross-sections

were compatible with the SM values within the uncertainties and were used to place constraints on the Wilson coefficients, $c_i$, of 5 CP-even dimension-6 operators. The results were also compatible with the SM predictions within uncertainties.

A study of angular observables in $VH(V = W, Z)$ production, sensitive to anomalous components in the $HVV$ vertex, was performed in Ref. [5], exploiting the fact that the different anomalous Spin/CP components in the $HVV$ vertex will have different effects on the angular distributions of the decay products of the vector boson. It was done using fast simulation based on `Delphes` and taking into account three of the main backgrounds: $t\bar{t}$, single top quark production and $W+$jets. The set of angular observables defined in this work was built to allow distinction between SM and anomalous components and also between different anomalous components, with the added feature of being linearly sensitive to the coupling of the CP-odd component. A likelihood analysis was performed in order to quantify the luminosity required to have a measurement compatible with the SM at the 95% confidence level and at $3\sigma$ level, for different anomalous components. It showed that using one of the presented variables, the hypothesis of an anomalous CP-odd component could be excluded at 95% confidence level with 100 $\text{fb}^{-1}$ of integrated luminosity. An asymmetry parameter based on the same variable was tested, observing a zero value for SM signal and backgrounds, as well as for signals with anomalous CP-even components, observing also a non-zero value for samples with anomalous CP-odd components, which increases with the value of the coupling.

The ATLAS Collaboration announced the first observation of $VH(V = W, Z)$ associated production [6], by combining an analysis of this production process in the $H \to b\bar{b}$ decay channel at a $\sqrt{s} = 13$ TeV, with previous ATLAS analyses targetting other decay channels, done in Run-1 and Run-2 of the LHC. The signal strengths obtained for the different decay channels and their combination were compatible with their SM expectation, within the uncertainties, which are of the order of 20% for the combined measurement. The $VH(H \to b\bar{b})$ analysis was also combined with previous analyses targetting the $H \to b\bar{b}$ decay in $VH$ and other production modes, leading to the first observation of the $H \to b\bar{b}$ decay, also achieved by the CMS Collaboration [7]. The signal strengths obtained for the different production modes and for their combination were also compatible with their SM values within the uncertainties, which are also of the order of 20% for the combined measurement.

Taking Refs. [5] and [6] as starting points, the $HWW$ interaction is studied by analyzing the associated production of a $W$ boson and a Higgs boson in the high transverse momentum (boosted) regime in order to have increased sensitivity to anomalous components. Despite having a low cross-section $\sigma_{WH} = 1.37$pb, $WH$ associated production has the advantage of allowing to probe the $HWW$ vertex independently of the $HZZ$ vertex, since one can identify the charge of the vector boson from the total charge of its decay products. The main disadvantage is that, even when targeting the $H \to b\bar{b}$ decay which has the highest branching ratio, $BR(H \to b\bar{b}) = 58.24\%$, the product of the cross-section and branching ratio is still very low, when compared to other production mechanisms such as gluon or vector boson fusion, which have higher cross-sections. This analysis targets the Higgs decay to a pair of $b$ quarks and the decay of the $W$ boson to an electron or muon and a neutrino.

The main objectives for this work are the optimization of the analysis procedure, the study of the sensitivity to the SM signal, and the study of the sensitivity to anomalous Spin/CP components in the $HWW$ vertex. The latter is done in two ways: first, by determining the changes to the expected signal strength, defined as the ratio between the expected signal yield with different anomalous components and the expected yield in the SM; second, by extending that measurement with a set of angular observables.

## 2. Theoretical Background

The SM $HWW$ interaction vertex is written in Equation 1.

$$i\Gamma^{\mu\nu}_{HWW} = ig_{HWW}g^{\mu\nu} = i\,(g_2 m_W)\,g^{\mu\nu}, \quad (1)$$

where $g_2$ is the $SU(2)$ coupling constant, $m_W$ is the mass of the $W$ boson and $g^{\mu\nu} = diag\,(+,-,-,-)$ is the Minkowski metric.

Modifications to the $HWW$ vertex are done in the framework of effective field theory techniques [8], a model-independent approach, which consists of extending the SM Lagrangian with higher-dimensional operators (mass dimension $> 4$) built from combinations of SM fields, supressed by increasing powers of the new physics scale, $\Lambda$. Two dimension-6 operators are taken into account, one CP-even, defined in Equation 2, and one CP-odd, defined in Equation 3.

$$\mathcal{O}_{WW} = \frac{g_2^2 b_{WW}}{4\Lambda^2}\Phi^\dagger\Phi W^a_{\mu\nu}W^{a\mu\nu} \quad \text{(CP-even)} \quad (2)$$

$$\tilde{\mathcal{O}}_{WW} = \frac{g_2^2 c_{WW}}{4\Lambda^2}\Phi^\dagger\Phi W^a_{\mu\nu}\tilde{W}^{a\mu\nu}, \quad \text{(CP-odd)} \quad (3)$$

where $\Phi$ is the SM Higgs doublet and $W^{\mu\nu}$ is the gauge field tensor. $\tilde{W}^{\mu\nu}$ is the dual field

tensor, given by $\epsilon^{\mu\nu\rho\sigma}W_{\rho\sigma}$, where $\epsilon^{\mu\nu\rho\sigma}$ is the (antisymmetric) Levi-Civita tensor, and $b_{WW}$ and $c_{WW}$ are the Wilson coefficients, that parametrize the relative strength of the two operators. These addition of these operators to the SM $HWW$ vertex leads to the modified interaction vertex in Equation 4, following the parametrization of Ref. [5].

$$\begin{aligned} i\Gamma^{\mu\nu}_{HWW}(k_1,k_2) &= i(g_2 m_W) \\ &\left[g^{\mu\nu}\left(1+a_W-\frac{b_{W1}}{m_W^2}(k_1\cdot k_2)\right)\right. \\ &\left.+\frac{b_{W1}}{m_W^2}\,k_1^\nu k_2^\mu+\frac{c_W}{m_W^2}\epsilon^{\mu\nu\rho\sigma}k_{1_\rho}k_{2_\sigma}\right] \end{aligned} \tag{4}$$

where $(1+a_W)$ is a scaling factor to allow possible rescalings of the SM contribution. $b_{W1}=\frac{2m_W^2 b_{WW}}{\Lambda^2}$ and $c_W=\frac{2m_W^2 c_{WW}}{\Lambda^2}$ are functions of the Wilson coefficients, defined in a way to remove $\Lambda$ from the set of independent variables, and $k_1$ and $k_2$ are the gauge boson momenta. Here, two anomalous components are identified, a CP-even one, with coupling $b_{W1}$, and a CP-odd one, with coupling $c_W$.

## 3. Experimental apparatus

### 3.1. Large Hadron Collider

The Large Hadron Collider is the most powerful particle accelerator in the world and is based at CERN (European Organization for Nuclear Research), in Geneva, Switzerland. It is a 27 kilometer ring, which uses a set of radiofrequency cavities to accelerate two beams of protons in opposite directions, up to an energy of 6.5 TeV each, colliding them at a frequency $f_{coll}=40$ MHz. Data used for this work were collected during Run 2 of the LHC, (from 2015 to 2018) at a center-of-mass energy $\sqrt{s}=13$ TeV, with 30 to 40 simultaneous interactions per bunch crossing.

### 3.2. ATLAS detector

The ATLAS detector [9] is a general-purpose apparatus with a forward-backward symmetric cylindrical geometry and an almost $4\pi$ coverage of the solid angle around the collision point. The reference system used is a right-handed coordinate system with its origin on the interaction point, the $x$ direction pointing at the center of the LHC, the $y$ direction pointing upwards and the $z$ (longitudinal) direction pointing along the beam pipe. One can also use a set of cylindrical coordinates: $\phi$, the azimuthal angle in the $xy$ (transverse) plane, and $\theta$, the polar angle from the beamline. The pseudorapidity variable, $\eta$, defined as $\eta=-\ln\tan(\theta/2)$, is frequently used instead of the polar angle $\theta$.

The ATLAS detector is composed of an inner tracking detector (ID), covering a pseudorapidity range $|\eta|<2.5$, surrounded by a thin superconducting solenoid which generates a 2T axial magnetic field. A high-granularity liquid argon/steel sampling calorimeter performs electromagnetic energy measurements for $|\eta|<3.2$. A steel/scintillator tile calorimeter performs hadronic energy measurements for $|\eta|<1.7$, complemented by a liquid argon/copper calorimeter for $1.5<|\eta|<3.2$. In the forward region, $3.2<|\eta|<4.9$, a liquid argon/copper/tungsten calorimeter performs electromagnetic and hadronic energy measurements. The muon spectrometer covers the pseudorapidity range $|\eta|<2.7$ and is tasked with performing precise measurements of muon trajectories and trigger on events with muons. It has a set of toroidal magnets in the barrel and endcaps, which provide additional bending of muon trajectories along $\phi$, improving the precision in momentum measurement compared to tracker-only measurements.

The several detector components are connected to a two-level trigger system, which decides in real-time whether or not to record an event in permanent storage for further analysis. It is divided in two levels: the hardware-based Level 1 (L1) trigger and the software-based High Level Trigger, which in combination, select about one thousand out of the forty million events that occur each second.

## 4. Analysis

This analysis targets events where the $W$ boson has a transverse momentum larger than 250 GeV and decays to an electron or muon and a neutrino, with the Higgs boson decaying to a pair of $b$-quarks. This final state, schematized in Figure 1, is defined by the presence of missing transverse energy from the neutrino and an isolated electron or muon with high transverse momentum from the decay of the $W$ boson, which allows efficient triggering in the presence of a large multijet background. The Higgs boson is reconstructed as a large-$R$ jet with two $b$-tagged subjets, since the very large Lorentz boost causes the $b$-quarks from the decay to become very collimated, which leads to a drop in efficiency if the Higgs is identified using two *resolved* $b$-jets, as was done for previous studies of this channel [6, 7].

The main backgrounds in this analysis are associated production of a $W$ boson with jets ($W+$jets), top quark pair production ($t\bar{t}$), single top quark production in the $Wt$ channel and $WZ$ production.

### 4.1. Data and simulated samples

The proton-proton collision data used in this analysis were collected by the ATLAS detector during the Run-2 of the LHC, which, after a set of data quality requirements, corresponds to an

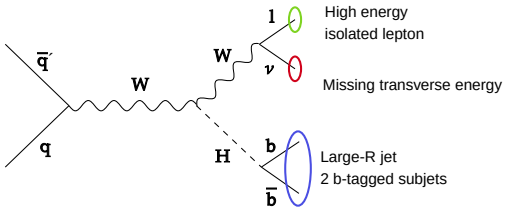


Figure 1: Schematic representation of the event topology of boosted $WH \to \ell\nu b\bar{b}$ events.

integrated luminosity of $139.9 \pm 2.4$ fb$^{-1}$at a center-of-mass energy $\sqrt{s} = 13$ TeV.

The simulated samples of SM signal and backgrounds were generated using the `Geant4`-based ATLAS Simulation Infrastructure [10] for the detector description where the interaction of the particles with each of the detector components is simulated very accurately. The set of simulated detector responses is given as input to the same set of reconstruction and pile-up removal algorithms that run on data, in order to approximate them as much as possible. The cross-sections used to normalize the different processes at $\sqrt{s} = 13$ TeV are given on Table 1.

BSM signal samples for the studies of the sensitivity to anomalous Spin/CP components in the $HWW$ interaction vertex were generated at LO in QCD for $\sqrt{s} = 14$ TeV with `Madgraph5_aMC@NLO` [11], using as input model an implementation of the the extended interaction vertex defined in Equation 4. These samples were generated with the $W$ boson decaying to electrons or muons (no $\tau$ leptons) and two filters were applied on the generator-level lepton, $p_T > 20$ GeV and $|\eta| < 3$ (with an efficiency of $\approx$ 80%), due to the negligible acceptance of the analysis outside of this phase space. Detector simulation was done using using `Delphes3` [12] with a modified version of the default ATLAS card, with analysis-specific reconstruction criteria. Table 2 shows the anomalous components (and couplings) used to generate the different samples, and the (filtered) cross-sections. The uncertainty on the cross-sections is derived in `Madgraph5_aMC@NLO` and comes mainly from PDF uncertainties.

All of the generated samples include the effect of pile-up, achieved by overlaying minimum bias events.

### 4.2. Object reconstruction

Large-$R$ jets are reconstructed using the anti-$k_t$ algorithm with a radius parameter ($R = 1.0$), in order to fully contain the decay products. These also undergo a *trimming* [13] procedure, which removes low-energy deposits inside them, generally associated with pile-up and underlying event contamination. The trimming parameters are $R_{sub} = 0.2$ and $f_{cut} = 0.05$. In order to improve its resolution, the large-$R$ jet invariant mass is calculated using a weighted combination of tracker and calorimeter information. The $b$-quarks from the $H \to b\bar{b}$ decay are identified using track jets, built using variable-radius reconstruction, in which the radius of the jet is inversely proportional to its transverse momentum, leading to a better reconstruction efficiency across a larger transverse momentum range. The reconstruction parameters are $\rho = 30$ GeV, $R_{min} = 0.02$ and $R_{max} = 0.4$. These are then matched to the leading large-$R$ jet via ghost-association [14], defining subjets as the set of track jets which are ghost-associated to the highest transverse momentum (leading) large-$R$ jet.

### 4.3. Event selection and categorization

A set of conditions is applied to data, to remove events which may have been poorly reconstructed: the event should have happened in a period in which all ATLAS subdetectors were operational and providing good quality data and, in addition, it should have a primary vertex. A set of event selection criteria are applied in order to remove background and pile-up contamination:

1. recorded using single electron triggers in the electron channel and missing transverse energy triggers in the muon channel
2. exactly one isolated, high transverse momentum lepton
3. missing transverse energy ($E_{\mathrm{T}}^{\mathrm{miss}}$) $> 30$ GeV
4. transverse momentum of the $W$ boson, $p_{T_W} >$ 250GeV, obtained from the vectorial sum of the missing transverse energy and the transverse momentum of the lepton
5. at least one trimmed large-$R$ jet with $p_T >$ 250 GeV and $|\eta| < 2.0$
6. at least two subjets, with $p_T > 10$ GeV and $|\eta| < 2.5$
7. two leading subjets must be $b$-tagged, with the MV2c10 algorithm in the 70% efficiency working point
8. invariant mass of the large-$R$ jet higher than 50 GeV
9. absolute difference between the rapidity of the $W$ boson and Higgs boson candidate of $|\Delta y(W, H)| < 1.4$

The boosted Higgs boson tagging strategy is optimized for the SM signal, defining the optimal track jet reconstruction technique and $b$-tagging

| Process | Generator | $\sigma \times BR$ [pb] (order) |
|---|---|---|
| Signal | | |
| $qq \to WH \to l^+\nu bb$ | `Powheg MiNLO`, `Pythia8` | 0.1646 (NNLO QCD, NLO EW) |
| $qq \to WH \to l^-\nu b\bar{b}$ | `Powheg MiNLO`, `Pythia8` | 0.1045 (NNLO QCD, NLO EW) |
| Backgrounds | | |
| $W+$jets, $W \to l\nu$ | `Sherpa 2.2.1` | $183600 \times 0.325$ (NNLO QCD) |
| $t\bar{t}$ non-fully-hadronic | `Powheg-BOX`, `Pythia8` | $831.76 \times 0.543$ (NNLO+NNLL QCD) |
| Single-top $Wt$ | `Powheg-BOX`, `Pythia8` | $71.7 \times 1$ (NLO QCD) |
| $qq \to WZ \to l\nu qq$ | `Sherpa 2.2.1` | $50.3 \times 0.227$ (NLO QCD $\leq 1j$, LO QCD $\geq 2j$) |

Table 1: ATLAS simulated samples generated for the SM signal and background processes, generator used, cross section times branching ratio $\sigma \times BR$ used to normalize the different processes at $\sqrt{s} = 13\,\text{TeV}$, and the order of cross-section calculation. Here, $l = e, \mu, \tau$. Branching ratios correspond to the decays shown.

| Couplings | $\sigma \times BR$ [fb] |
|---|---|
| $a_w = 0$ (SM-like) | $151.4 \pm 0.4$ |
| $a_w = 0, b_{w1} = 0.05$ | $211.7 \pm 0.7$ |
| $a_w = 0, b_{w1} = 0.1$ | $275.1 \pm 0.9$ |
| $a_w = 0, c_w = 0.05$ | $154.1 \pm 0.4$ |
| $a_w = 0, c_w = 0.1$ | $159.9 \pm 0.5$ |

Table 2: BSM samples and cross section times branching ratio (BR) used to normalise the different processes at 13 TeV. $b_{w1}$ ($c_w$) is the coupling of the CP-even (CP-odd) component, defined in Equation 4. The uncertainty on the cross-sections is derived in `Madgraph5_aMC@NLO` and comes from PDF uncertainties.

selection, using as figure of merit the median (statistical) significance, $Z_{med}$, defined in [15] as $Z_{med} = \sqrt{2\,(s+b)\,ln\,(1+s/b) - s}$, where $s$ and $b$ are the expected signal and background yields, respectively (derived from MC samples).

| | Fixed-radius | Variable-radius |
|---|---|---|
| Efficiency (%) | 43.7 | 39.1 |
| $t\bar{t}$ rejection factor | 100.0 | 142.9 |
| $W+$jets rejection factor | 184.3 | 219.5 |
| $Z_{med}$ | 0.861 | 0.898 |

Table 3: Higgs tagging efficiencies, rejection factors for $t\bar{t}$ and $W+$jets production and median significance for fixed-radius and variable-radius track jets.

The adoption of the $|\Delta y(W,H)|$ selection criteria is also studied, taking into account the SM signal, and the results are given in Table 5, using as figure of merit the expected significance, $Z_{exp}$, obtained from the global fit described in Section 4.4, taking into account statistical uncertainties only.

| | Two leading subjets | All subjets |
|---|---|---|
| Efficiency (%) | 39.1 | 42.6 |
| $t\bar{t}$ rejection factor | 142.9 | 83.3 |
| $W+$jets rejection factor | 219.5 | 144.5 |
| $Z_{med}$ | 0.898 | 0.766 |

Table 4: Higgs tagging efficiencies, rejection factors for $t\bar{t}$ and $W+$jets production and median significance for both tagging strategies using variable-radius track jets

#### 4.3.1 Event categorization

Given that the sensitivity to anomalous components is expected to increase with energy, the selected events are divided in two $p_{T_W}$ regions: a medium $p_{T_W}$ region with 250 GeV $< p_{T_W} <$ 400 GeV , and a high $p_{T_W}$ region with $p_{T_W} >$ 400 GeV , chosen to match the Simplified Template Cross Section binning recommendations in Ref. [16].

The number of $b$-tagged track jets with $p_T > 10\,\text{GeV}$ which are not matched to the leading large-$R$ jet is used to categorize the events into a signal region and a top control region. The signal (control) region contains events with zero (at least one) additional $b$-tagged track jets outside the large-$R$ jet.

The number of small-$R$ jets, i.e. anti-$k_t$ $R = 0.4$ calorimeter jets with $p_T > 30$ GeV, which have $\Delta R\,(\text{small-R jet}, \text{large-}R\text{ jet}) > 1.0$ is used to split the events in the signal region into high low purity regions. The high (low) purity signal region contains zero (at least one) additional small-$R$ jets.

### 4.4. Statistical analysis methodology

The parameter of interest to be extracted is the signal strength, $\mu$, defined as the ratio between the observed and expected yields (derived from simulation). This is done via a binned likelihood fit to the distribution of the invariant mass of the leading (highest transverse momentum) large-$R$ jet in all the analysis regions simultaneously. The $p$-

| | No cut | $\lvert\Delta y(W,H)\rvert < 1.4$ | **Difference (%)** |
|---|---|---|---|
| Signal yields | 97.53 ± 9.88 | 91.94 ± 9.59 | -5.7 |
| Background yields | 5913.05 ± 76.90 | 4695.9 ± 68.53 | -20.6 |
| $Z_{exp}$ | 2.56 | 2.67 | 4.3 |

Table 5: Yields for signal and background in the signal region and expected significance before and after the requirement of an upper limit $|\Delta y(W,H)| < 1.4$. Statistical uncertainties on the yields are shown.

*value*, $p$, quantifies the compatibility between the background-only hypothesis ($\mu = 0$) and the data, and the statistical significance of the result, $Z$, is quoted in terms of (Gaussian) standard deviations as $Z = \Phi^{-1}(1-p)$, where $\Phi$ is the inverse of the Gaussian cumulative distribution function.

### 4.5. Study of the sensitivity to anomalous Spin/CP components

This section describes the methods used to study the sensitivity of the analysis developed in the previous section to anomalous components in the $HWW$ vertex, and uses the SM signal and background samples described in Table 1, with full ATLAS detector simulation and event reconstruction, and the BSM signal samples described in Table 2, with `Delphes` detector simulation and event reconstruction. After detector simulation and event reconstruction, the event selection and categorization criteria defined in Section 4.3 are applied to both samples, when possible (trigger selections are not implemented in Delphes).

#### 4.5.1 Signal strength-based studies

In order to determine the expected signal strength for BSM signals with anomalous components, the signal yields in the SM sample reconstructed using full ATLAS simulation (mentioned previously) are scaled by a factor $f = N_{BSM}/N_{SM}$, extracted from Delphes samples for each of the analysis regions. This assumes that anomalous components do not change the shape of the large-$R$ jet invariant mass distribution, and that the ratio between the acceptances for BSM and SM signals are similar for $\sqrt{s} = 13$ TeV and $\sqrt{s} = 14$ TeV.

#### 4.5.2 Angular observable studies

Anomalous CP-even and CP-odd components in the $HWW$ vertex lead to modifications to the expected signal strength. However, using only the signal strength, it is not possible to disentangle the contributions from different anomalous components, for which other observables are necessary. Following Ref. [5], the following angular observables are defined:

$$\cos\theta^* = \frac{\mathbf{p}_\ell^{(W)} \cdot \mathbf{p}_W}{|\mathbf{p}_\ell^{(W)}||\mathbf{p}_W|} \tag{5}$$

$$\Delta\phi^{lW} = \Delta\phi\left(\mathbf{p}_\ell^{(W)}, \mathbf{p}_W\right) \tag{6}$$

$$\cos\delta^+ = \frac{\mathbf{p}_\ell^{(W)} \cdot (\mathbf{p}_H \times \mathbf{p}_W)}{|\mathbf{p}_\ell^{(W)}||\mathbf{p}_H \times \mathbf{p}_W|} \tag{7}$$

$$\cos\delta^- = \frac{\left(\mathbf{p}_\ell^{(H-)} \times \mathbf{p}_\nu^{(H-)}\right) \cdot \mathbf{p}_W}{|\mathbf{p}_\ell^{(H-)} \times \mathbf{p}_\nu^{(H-)}||\mathbf{p}_W|}, \tag{8}$$

where $\mathbf{p}_\ell^{(W)}$ is the 3-momentum of the electron or muon in the $W$ boson rest frame and $\mathbf{p}_\ell^{(H-)}$ ($\mathbf{p}_\nu^{(H-)}$) is the 3-momentum of the electron or muon (neutrino) in the rest frame of a Higgs boson with $\mathbf{p} = -\mathbf{p}_H$. All other 3-momenta are defined in the lab frame.

A comparison between the different signals and backgrounds after event reconstruction and application of the event selection criteria defined in Section 4.3 is carried out, which requires that `Delphes` and full ATLAS detector simulation and event reconstruction be as similar as possible. For this purpose, a reweighting of the `Delphes` samples is carried out, such that the acceptance and reconstruction effects from ATLAS samples are taken into account. The decision was to reweight the samples based on the transverse momentum of the signal lepton in each of the analysis regions, which gives the best post-reweighting agreement (closure) for the angular observable distributions, showing deviations lower than 20% for the $\cos\theta^*$and $\cos\delta^+$distributions for 250 GeV $< p_{T_W} <$ 400 GeV .

In Figure 2, it can be seen that for the observable $\cos\theta^*$, the SM signal distribution is symmetric around 0 and the BSM signal distributions are skewed to higher values, in agreement with the truth-level analysis. Furthermore, it can also be seen that the background distributions are skewed to lower values. This leads to the conclusion that, even after full event reconstruction and selection and taking backgrounds into account, this variable is able to distinguish between SM signal, backgrounds and BSM signals.

Figure 3 shows the shape of the $\cos\delta^+$distribution for the SM signal, a BSM signal with an anomalous

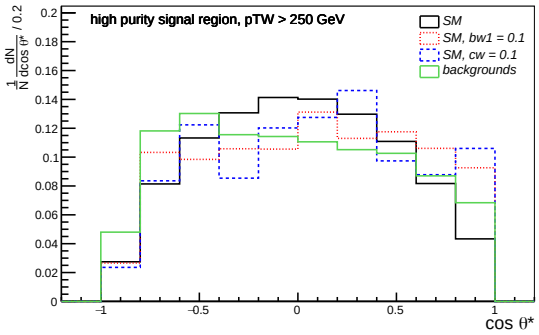


Figure 2: Comparison of the (unit area) shape of the $\cos\theta^*$distributions for the SM (solid black), SM+CP-even component (dashed red), SM+CP-odd (dashed blue) and backgrounds (green)

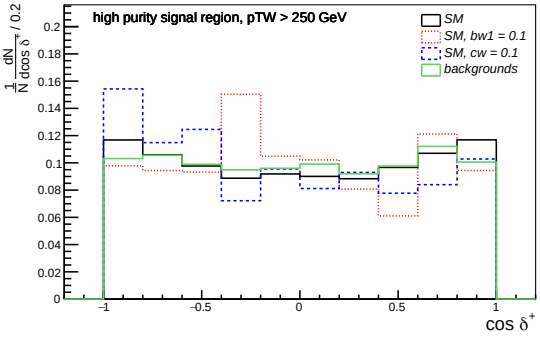


Figure 3: Comparison of the (unit area) shape of the $\cos\delta^+$distributions for the SM (solid black), SM+CP-even component (dashed red), SM+CP-odd (dashed blue) and backgrounds (green)

CP-even component, a BSM signal with an anomalous CP-odd component, and backgrounds. Here, it can be seen that the distribution for the SM signal is symmetric around 0 and for the BSM sample with a CP-odd component, it is skewed to the left, in agreement with the truth-level analysis, the distribution for backgrounds also being symmetric around 0. For the BSM sample with a CP-even component, it is asymmetric, in disagreement with the truth-level analysis, but containing large fluctuations, which is most likely due to the small number of generated events for these samples and the fact that the acceptance is smaller for this sample than for the BSM sample with a CP-odd component, thus leading to larger fluctuations.

Figure 4 shows the shape of the $\cos\delta^+$distribution for the SM signal, two BSM signals with an anomalous CP-odd components with increasing value of the coupling, and backgrounds. It shows that the distribution of for the BSM sample with

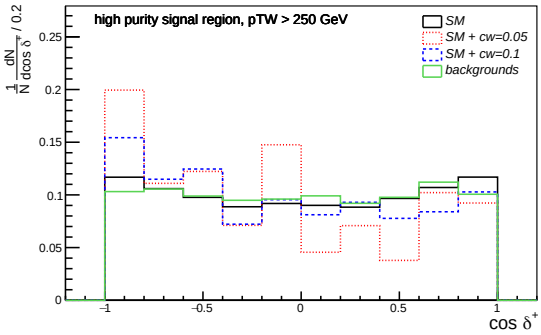


Figure 4: Comparison of the (unit area) shape of the $\cos\delta^+$distributions for the SM (solid black), SM+CP-odd component with increasing values of the coupling (dashed red and dashed blue) and backgrounds (green).

a CP-odd component with a lower value of the coupling, $c_w = 0.05$, seems more asymmetric than that for the sample with the higher value of the coupling, $c_w = 0.1$, contradicting the conclusion of the truth-level analysis. This is believed to be due to large fluctuations, similar to what is seen in Figure 3.

A data-MC comparison of the distributions of the different angular observables in the top control region for each of the $p_{T_W}$regions is carried out, in order to verify if these are properly modelled in the ATLAS simulation, so that they can be used in future ATLAS analyses. The comparison plots for the 250 GeV $< p_{T_W} <$ 400 GeV region are shown in Figures 5 and 6 for the observables $\cos\theta^*$and $\cos\delta^+$, respectively. In these figures, it can be seen that the data-MC ratio floats around unity, with most of the differences likely covered by statistical fluctuations. Similar conclusions are drawn for $p_{T_W} >$ 400 GeV , but with larger fluctuations.

## 5. Results

### 5.1. Sensitivity to the SM Higgs boson signal

To determine the sensitivity to the SM signal, the expected signal strength ($\mu_{exp}$) and significance ($Z_{exp}$) for 139 fb$^{-1}$ of proton-proton collisions at $\sqrt{s} = 13$TeV are calculated using the fit described in Section 4.4, without taking into account systematic uncertainties. The expected signal strength is $\mu_{exp} = 1.00 \pm 0.41$ with an expected significance, $Z_{exp} = 2.52\sigma$. Taking into account all of the systematic uncertainties, one obtains $\mu_{exp} = 1.0 \pm 0.62$ and $Z_{exp} = 1.91$, not enough to constitute evidence for the independent observation of boosted $WH$ production. The uncertainty is dominated by the low data statistics, followed by uncertainties on large-$R$ jet quantities [17].

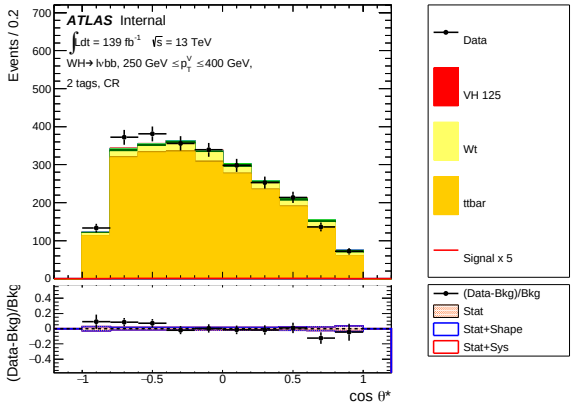


Figure 5: Data-MC comparison plots for the $\cos\theta^*$angular variable in the top control region for medium (left) and high (right) $p_{T_W}$regions

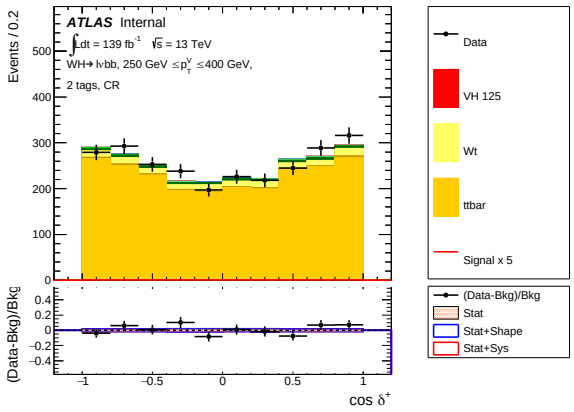


Figure 6: Data-MC comparison plots for the $\cos\delta^+$angular variable in the top control region for medium (left) and high (right) $p_{T_W}$regions

## 5.2. Sensitivity to anomalous Spin/CP components

### 5.2.1 Signal strength-based studies

The values of the expected signal strength and significance for 139 fb$^{-1}$ of proton-proton collisions at $\sqrt{s}$ = 13 TeV for the different BSM signals, obtained with the procedure described in Section 4.4 and not taking into account systematic uncertainties, are given in Table 6, with the SM values also shown for comparison purposes. In the second and third lines of this table, it can be seen that the expected signal strengths for samples with an anomalous CP-even component are much larger than the one obtained for the SM sample, showing that this analysis is sensitive even to small values of the coupling. In the fifth line, one can also see that this analysis is sensitive to a signals with an anomalous CP-odd component with a large coupling, $c_w = 0.1$. This happens because, even though the change in the cross-sections induced by these components is very small, the modification in the acceptance is larger than that for CP-even ones. Finally, in the third line, it can be seen that, for a CP-odd component with a small value of the coupling, such as $c_w = 0.05$, the expected signal strength is very similar to that obtained for the SM sample. This means that the signal strength measurements alone are not sensitive to CP-odd components with small couplings, and that additional observables are necessary.

| Signal samples | $\mu_{exp}$ | $Z_{exp}(\sigma)$ |
|---|---|---|
| SM | 1.00 ± 0.41 | 2.52 |
| SM + $b_{w1} = 0.05$ | 2.60 ± 0.44 | 6.49 |
| SM + $b_{w1} = 0.1$ | 6.82 ± 0.51 | 15.90 |
| SM + $c_w = 0.05$ | 1.54 ± 0.42 | 4.04 |
| SM + $c_w = 0.1$ | 3.05 ± 0.45 | 7.78 |

Table 6: Expected signal strengths and significances for the SM signal and for BSM signals, in which the SM $HWW$ vertex is supplemented with a set of (anomalous) components. $b_{w1}$ is the coupling of the CP-even component and $c_w$ is the coupling of the CP-odd component.

### 5.2.2 Angular observable studies

The asymmetry in the observable $\cos\delta^+$, defined in Equation 9, shown to be sensitive to the existence of anomalous components, is calculated for the the SM signal and background samples, as well as for the different BSM samples (assuming perfect background subtraction), after detector simulation, event reconstruction, selection and categorization, and is shown in Table 7.

$$A(\cos\delta^+) = \frac{N(\cos\delta^+ > 0) - N(\cos\delta^+ < 0)}{N(\cos\delta^+ > 0) + N(\cos\delta^+ < 0)} \quad (9)$$

The calculated values of the asymmetry are compatible with zero for the SM signal and backgrounds, while non-zero values are obtained for samples with anomalous components, despite the large statistical uncertainties in the simulated samples used to derive these results. This leads to the conclusion that the asymmetry defined in Equation 9 can potentially increase the sensitivity of this analysis to CP-odd components with small couplings with regards to the sensitivity obtained from signal strength measurements alone. Nonetheless, contrary to what is expected from the truth-level analysis, this observable is not symmetric in samples with anomalous CP-even components due to statistical fluctuations. Given that the equivalent generated luminosity for each of the BSM samples is larger than 139 fb$^{-1}$, similar

or worse fluctuations are expected for the Run-2 integrated luminosity, leading to the conclusion that higher instantaneous luminosities are needed to clearly distinguish between CP-even and CP-odd anomalous components using this observable. To improve the sensitivity, a global fit that combines the information from several variables could be used.

| Samples | Asymmetry |
|---|---|
| Backgrounds | 0.003 ± 0.028 |
| SM | -0.002 ± 0.133 |
| SM + $b_{w1} = 0.05$ | 0.142 ± 0.087 |
| SM + $b_{w1} = 0.1$ | -0.081 ± 0.055 |
| SM + $c_w = 0.05$ | -0.319 ± 0.112 |
| SM + $c_w = 0.1$ | -0.123 ± 0.082 |

Table 7: Asymmetry of the $\cos\delta^+$distribution in the high purity signal region for $p_{T_W} > 250\,\text{GeV}$, for the ATLAS SM signal and backgrounds (described in Table 1) as well for different BSM signals (described in Table 2). Statistical uncertainties shown.

## 6. Conclusions

This work explored the sensitivity of $WH \to \ell\nu b\bar{b}$ associated production channel in the boosted regime, $p_{T_W} > 250$ GeV, to anomalous Spin/CP components in the $HWW$ vertex, with the full LHC Run-2 dataset, corresponding to a total integrated luminosity, $L = 139.9 \pm 2.4$ fb$^{-1}$ at a center-of-mass energy of $\sqrt{s} = 13\,\text{TeV}$. It targeted the decay of the $W$ boson to an electron or muon and a neutrino and the decay of the Higgs boson to a pair of $b$-quarks. Given that, in this regime, these $b$-quarks are very collimated, the Higgs boson was identified using a trimmed anti-$k_t$, $R = 1.0$ jet with a substructure compatible with a $H \to b\bar{b}$ decay.

The analysis procedure was optimized, using the SM signal as reference. The strategy for identification of boosted $H \to b\bar{b}$ decays was optimized, concluding that the optimal strategy is to reconstruct variable-radius track jets, match them to the leading large-$R$ using ghost-association and selecting the two leading associated track jets for $b$-tagging, in order to identify the $b$-quarks from the decay. A selection criteria on the absolute rapidity difference between the reconstructed $W$ and the Higgs candidate, $|\Delta y(W, H) < 1.4|$, was introduced in the analysis in order to improve signal and background separation.

The sensitivity to the SM signal was obtained, taking only statistical uncertainties into account. The expected signal strength is $\mu_{exp} = 1.00 \pm 0.45$, corresponding to an expected significance $Z_{exp} = 2.52\sigma$, while considering also account the full set of experimental and modelling systematic uncertainties, these become $\mu_{exp} = 1.0 \pm 0.62$ and $Z_{exp} = 1.91$, with the uncertainty being dominated by the low data statistics, followed by uncertainties on large-$R$ jet quantities, such as energy scale or resolution. The significance is not high enough to claim observation of SM $WH$ production, given that the high energy regime targeted by this analysis contains less than 2% of the total SM production cross-section.

The sensitivity of the $WH \to \ell\nu b\bar{b}$ channel to anomalous components in the $HWW$ vertex was studied using simulated samples in which the SM vertex is supplemented by CP-even or CP-odd components, with a set of benchmark values of its couplings, and taking only statistical uncertainties into account. For signals with anomalous CP-even components, $\mu_{exp} = 2.60 \pm 0.44$ with an expected significance $Z_{exp} = 6.49$ (for $b_{w1} = 0.05$) and $\mu_{exp} = 6.82 \pm 0.51$, with an expected significance $Z_{exp} = 15.90$ (for $b_{w1} = 0.1$), which are not compatible the values expected for the SM signal, showing that this channel is sensitive to CP-even components using only signal strength measurements. For a signal with an anomalous CP-odd component with coupling $c_w = 0.1$, the expected signal strength is $\mu_{exp} = 3.05 \pm 0.45$, corresponding to an expected significance of $Z_{exp} = 7.78$, which is also not compatible with the value expected for the SM signal, demonstrating that this channel is sensitive to anomalous CP-odd components with large values, using only measurements of the signal strength. These are optimistic results, since systematic uncertainties are not taken into account. For signals with an anomalous CP-odd component with small couplings, the expected signal strength is compatible with the value obtained for the SM signal, leading to the conclusion that this channel is not sensitive to anomalous CP-odd components with small couplings using only signal strength measurements. In addition, the signal strength is not enough to distinguish between anomalous components with different CP properties, and that other observables are required.

A study of angular observables proposed in Ref. [5] to distinguish not only between the backgrounds, the SM signal and signals with anomalous components but also between different anomalous components was carried out. It showed that, when taking into account full detector simulation and event reconstruction, as well as the full set of event selection and categorization criteria, the observable $\cos\theta^*$can distinguish between the SM signal and backgrounds and signals with anomalous components, and the observable $\cos\delta^+$has the potential to increase the sensitivity to anomalous CP-odd components with small couplings, but that higher luminosities than the ones currently

accumulated for the LHC Run 2 are necessary to distinguish between anomalous components with different CP properties. The modelling of these variables was also studied in the control regions of the analysis, comparing MC and data, observing a very good agreement, and demonstrating that they can be used in a future ATLAS analysis.

The next steps in this study would be to include these observables in the ATLAS analysis, using the full Run 2 luminosity with improved calibrations and simulations, and also explore methods to extract the value of the coupling using these variables, such as the calculation of asymmetry parameters, or multivariable methods to combine information from the signal strength and the different angular observables studied.

**Acknowledgements**

The author would like to thank Patricia Muiño and Rui Santos, for their trust and supervision, without which this work would not be possible. The author would like to thank the ATLAS Collaboration, and specially the boosted $VH(b\bar{b})$ analysis team. The author would also like to acknowledge the support of the Fundação para a Ciência e Tecnologia through the projects CERN/FIS-PAR/0008/2017 and CERN/FIS-PAR/0002/2019.

**References**

[1] Andrei D Sakharov. Violation of cp invariance,c asymmetry, and baryon asymmetry of the universe. *Soviet Physics Uspekhi*, 34(5):392–393, may 1991.

[2] Patrick Huet and Eric Sather. Electroweak baryogenesis and standard model cp violation. *Physical Review D*, 51(2):379–394, Jan 1995.

[3] CMS Collaboration. Constraints on anomalous HVV couplings from the production of Higgs bosons decaying to $\tau$ lepton pairs. *Physical Review D*, 100(11), Dec 2019.

[4] ATLAS Collaboration. Measurement of VH, $H \to b\bar{b}$ production as a function of the vector-boson transverse momentum in 13 TeV pp collisions with the ATLAS detector. *Journal of High Energy Physics*, 2019(5), May 2019.

[5] R. M. Godbole, D. J. Miller, K. A. Mohan, and C. D. White. Jet substructure and probes of CP violation in Vh production. *Journal of High Energy Physics*, 2015(4), Apr 2015.

[6] ATLAS Collaboration. Observation of H$\to b\bar{b}$ decays and VH production with the ATLAS detector. *Physics Letters B*, 786:59–86, Nov 2018.

[7] CMS Collaboration. Observation of Higgs Boson Decay to Bottom Quarks. *Physical Review Letters*, 121(12), Sep 2018.

[8] Ilaria Brivio and Michael Trott. The standard model as an effective field theory. *Physics Reports*, 793:1–98, Feb 2019.

[9] ATLAS Collaboration. The ATLAS experiment at the CERN large hadron collider. *Journal of Instrumentation*, 3(08):S08003–S08003, aug 2008.

[10] ATLAS Collaboration. The atlas simulation infrastructure. *The European Physical Journal C*, 70(3):823–874, Sep 2010.

[11] J. Alwall, R. Frederix, S. Frixione, V. Hirschi, F. Maltoni, O. Mattelaer, H.-S. Shao, T. Stelzer, P. Torrielli, and M. Zaro. The automated computation of tree-level and next-to-leading order differential cross sections, and their matching to parton shower simulations. *Journal of High Energy Physics*, 2014(7), Jul 2014.

[12] J. de Favereau, C. Delaere, P. Demin, A. Giammanco, V. Lemaître, A. Mertens, and M. Selvaggi. Delphes 3: a modular framework for fast simulation of a generic collider experiment. *Journal of High Energy Physics*, 2014(2), Feb 2014.

[13] David Krohn, Jesse Thaler, and Lian-Tao Wang. Jet trimming. *Journal of High Energy Physics*, 2010(2), Feb 2010.

[14] Matteo Cacciari, Gavin P Salam, and Gregory Soyez. The catchment area of jets. *Journal of High Energy Physics*, 2008(04):005–005, Apr 2008.

[15] Glen Cowan, Kyle Cranmer, Eilam Gross, and Ofer Vitells. Asymptotic formulae for likelihood-based tests of new physics. *The European Physical Journal C*, 71(2), Feb 2011.

[16] LHC Higgs Cross Section Working Group. Handbook of LHC Higgs Cross Sections: 4. Deciphering the Nature of the Higgs Sector. Oct 2016.

[17] ATLAS Collaboration. Measurement of the associated production of a Higgs boson decaying to b quarks with a vector boson at high transverse momentum in pp collisions at 139 fb$^{-1}$ with the ATLAS detector (in preparation). Technical Report ATL-COM-PHYS-2019-1125, CERN, Geneva, Sep 2019.